Available online at www.sciencedirect.com

ScienceDirect

Mendeleev Commun., 2024, **34**, 802–804

Mendeleev Communications

Electronic structure and chemical bond in MdO_2

Yury A. Teterin,*[a,b] Mikhail V. Ryzhkov,[c] Andrei E. Putkov,[a,b] Konstantin I. Maslakov,[a] Anton Yu. Teterin,[b] Kirill E. Ivanov,[b] Stepan N. Kalmykov[a] and Vladimir G. Petrov[a]

[a] *Department of Chemistry, M. V. Lomonosov Moscow State University, 119991 Moscow, Russian Federation. E-mail: Teterin_YA@nrcki.ru*
[b] *National Research Center 'Kurchatov Institute', 123182 Moscow, Russian Federation*
[c] *Institute of Solid State Chemistry, Ural Branch of the Russian Academy of Sciences, 620990 Ekaterinburg, Russian Federation*

DOI: 10.1016/j.mencom.2024.10.011

The calculation of the electronic structure of MdO_2 was carried out using the fully relativistic method of discrete variation (RDV), a scheme of molecular orbitals (MO) was built and a histogram of the spectrum of X-ray photoelectron spectroscopy (XPS) was constructed in the range of electron binding energies (BE) 0–~40 eV. It was discovered that the complex structure of the XPS spectrum of valence electrons is associated with the formation of the outer valence molecular orbitals (OVMO, BE from 0 to ~15 eV) and of the inner valence molecular orbitals (IVMO, BE from ~15 to ~40 eV). The effective charge of Md in MdO_2 calculated from the MO compositions was equal to +0.50 electrons. IVMO electrons were found to weaken the bond formed by OVMO in MdO_2 by ~34%.

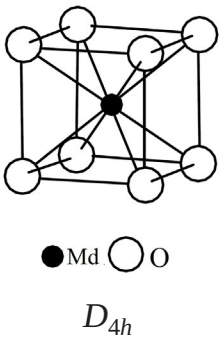

Keywords: MdO_2, chemical bond, electronic structure, XPS spectrum of valence electrons, relativistic method of discrete variation.

Among mendelivium isotopes, ^{258}Md ($T_{1/2}$ = 51.5 days, α-decay) is the longest-living one obtained in the particle accelerators. However, ^{256}Md ($T_{1/2}$ = 1.27 h, electron capture 90.7%, α-decay 9.3%) is most commonly used in chemical experiments because it can be produced on a larger scale. α-irradiation of micrograms of ^{253}Es can yield more than 10^6 ^{256}Md atoms per hour, which allows one to study some properties of Md ions and compounds.[1] The relativistic calculation of electron energies of the free Md atom was done.[2] The extrapolation of the experimental BEs of light actinide oxides allowed the estimation of Md core electron BEs.[3] The photoionization cross-sections for the ground and exited valence electronic states of mendelevium were obtained,[4] which was necessary for the calculation of MdO_2 XPS spectrum.

Much attention is paid to the study of the structure and other physicochemical properties of actinide compounds, in particular, actinoid oxides.[5–10] In the last years, the RDV method has been actively employed for the light actinides electronic structure calculations. These results are in a satisfactory agreement with the experimental XPS spectra of AnO_2.[11,12] This would suggest that the data of RDV calculations of the XPS spectrum of MdO_2 reflect the actual spectral structure.

This work aimed to study the chemical bonding nature in MdO_2, to determine the valence electronic density of states (DOS) and to draw an XPS spectrum of MdO_2 in the BE range from 0 to ~60 eV.

The MdO_8^{12-} (D_{4h}) cluster is a body-centered cube with Md in the center and eight oxygen ions in the corners with the interatomic distance $R_{Md–O}$ = 0.2267 nm (it was done by extrapolation of the experimental interatomic distances in light actinides dioxides). Here, the calculations of this cluster were carried out for the first time using the self-consistent field approximation of the relativistic discrete variation (RDV) method[13,14] based on the solution of Dirac–Slater equation for the 4-component spinors with the exchange-correlation potential.[15] The extended basis of atomic orbitals (AO) obtained by solving the Dirac–Slater equation for the isolated atoms included both the occupied and vacant Md $6d_{3/2}$, $6d_{5/2}$, $7p_{1/2}$ and $7p_{3/2}$ states. The basis also considers the cluster symmetry, *i.e.*, it employed the technique of projection operators[13] to build from the initial AOs their linear combinations transformed by the irreducible representations of the double D_{4h} group. To obtain these linear combinations, we employed an original symmetrization program using matrixes of the irreducible representations of the double point groups[15,16] and the transformation matrixes.[17] The numerical Diophantine integration for the calculation of the matrix elements of the secular equation was done by 22000 points distributed in the cluster space. This provided the convergence of the MO energies better than 0.1 eV. The absence of the muffin-tin (MT) potential approximation in the RDV method is its advantage inasmuch as there are no symmetry restrictions. Clusters of any types (*i.e.*, those without any symmetry) can be calculated with the equal accuracy. It is worth to note that the results of MO LCAO (molecular orbitals as linear combinations of atomic orbitals) calculations allow one to analyze directly the role of atomic states in the electronic structure, chemical bonding, spectral and other properties of solid compounds.

Neutral Md valence ground state configuration is $6s^26p^65f^{13}6d^07s^27p^0$, $^2F^0_{7/2}$. These electronic shells can participate in the MO formation in oxides.[11] The energies and

compositions of MOs in MdO_2 found in the RDV calculations are given in Table S1 in Online Supplementary Materials.

In the course of the chemical bonding formation, the valence MOs include the contributions from the Md 6*d* and 7*p* AOs, which are vacant in a neutral free Md atom. The Md 6*p*, 6*d* and 5*f* AOs contribute significantly to the MO formation, while the Md 6*s* AO is atomic and does not participate in the MO formation (see Table S1 in Online Supplementary Materials).

The highest occupied $26\gamma_6^-$ MO (HOMO) consists of 62% of the Md $5f_{7/2}$ and 38% of the O 2*p* AOs, at the top of the valence band the $22\gamma_7^-$ and $25\gamma_6^-$ MO containing 53% of the Md $5f_{7/2}$ and 44% of the O 2*p* AOs are observed. A relatively high Md 5*f* contributions in $18\gamma_6^-$, $15\gamma_7^-$ and $14\gamma_7^-$ MOs are also revealed at the OVMO bottom. The rest of the Md 5*f* electrons is delocalized mostly within the OVMO range. The delocalized Md 5*f* electrons increase the covalent component of the chemical bonding due to the overlap between Md 5*f* AO and oxygen orbitals. The MOs containing Md 6*d* AO appear at the OVMO bottom and in the IVMO range. Participation of the Md 5*f*, 6*d* and O 2*s*, 2*p* AOs in the MO formation agrees with the results obtained for the dioxides of more light actinides.[10,11,12] The covalent contribution from Md 5*f* AOs to the molecular orbitals of O 2*s*-type remains insignificant.

In MdO_2, as well as in other actinide oxides, the Md 6*p* AO participates both in the OVMO and IVMO formation. The Md $6p_{1/2}$–O 2*s* interaction is insignificant. A little involvement of the Md $6p_{1/2}$ in the IVMO formation is due to a relatively high Md $6p_{1/2}$, O 2*s* BEs differences. This induces the appearance of the 'antibonding' $17\gamma_6^-$, $13\gamma_7^-$ (5) and 'bonding' $15\gamma_6^-$, $11\gamma_7^-$ (8) IVMOs (see Table S1 in Online Supplementary Materials). The hybridization of the Md $6p_{1/2}$ and O 2*s* AOs in the 'antibonding' $16\gamma_6^-$ (7) and 'bonding' $14\gamma_6^-$ (9) IVMOs is insignificant in comparison with the corresponding orbitals in ThO_2.[18] This is due to the Md $6p_{1/2}$ BE growing compared with the O 2*s* one, which results in the decrease of the Md $6p_{1/2}$–O 2*s* interaction.

The covalence effects in MdO_2 are significant owing to the strong Md 6*d*–O 2*p* and Md 5*f*–O 2*p* overlapping.

These data form the basis for the MO scheme constructed for understanding the chemical bonding nature in MdO_2.

The difference in BE of the valence states and the Md $4f_{7/2}$ core level was used to build the MO scheme for MdO_2. The Md $4f_{7/2}$ BE obtained by extrapolation of the experimental An 4*f* BEs of actinide dioxides was found equal to 600.6 eV and the spin–orbit splitting was ΔE_{sl}(Md 4*f*) = 19.5 eV.

The experimental O 1*s* BE of 529.9 eV and the O 1*s*–O 2*s* BE difference of 508.3 eV[10,19] in AnO_2 were utilised in our simulations. Therefore, using 508.3 eV BE difference between O 1*s* and $12\gamma_7^-$ IVMO, we obtained $12\gamma_7^-$ IVMO BE of 21.60 eV. This agrees with the structure of experimental XPS spectra.

The vacant MOs in the scheme for MdO_2 are represented by dotted lines, the occupied MOs are shown as solid lines (Figure 1). The calculated MO energies are listed on the left side. The MO compositions (in %) are given above the lines. MO designations are specified on the right side (see Table S1 in Online Supplementary Materials), MO group number are given in parenthesis on the right. The valence-core BE differences are shown as vertical arrows. The BE differences (in eV) are indicated on the left. The value $\Delta E_{Md}{}^{T} = 576.3$ eV.[2]

In the scheme one can formally highlight the 'antibonding' $17\gamma_6^-$, $13\gamma_7^-$ (5) and $16\gamma_6^-$ (7) and the corresponding 'bonding' $15\gamma_6^-$, $11\gamma_7^-$ (8) and $14\gamma_6^-$ (9) IVMOs, as well as the 'quasiatomic' $12\gamma_7^-$ (6), $13\gamma_7^+$, $16\gamma_6^+$, $12\gamma_7^+$ and $15\gamma_6^+$ IVMOs formed mostly from the O 2*s* AO. The MO scheme clarifies the nature of chemical bonding in MdO_2 and allows the interpretation of the complex structures of other X-ray (electron, emission, absorption, conversion, *etc*.) spectra of MdO_2.

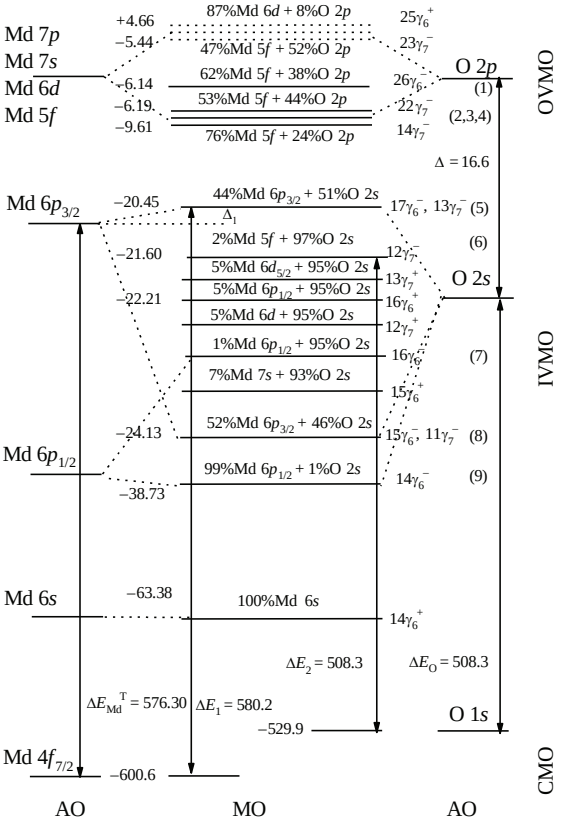

Figure 1 MO scheme for the MdO_8 cluster built taking into account the theoretical data. Arrows indicate some of the experimentally measurable BE differences. The calculated BEs (eV) are shown on the left side. The energy is not scaled. CMO is the core molecular orbital.

The Helius–Zigban model was used to obtain the valence XPS spectrum of MdO_2 (see Figure 2).[20] According to it, the intensity of the photoelectron line corresponding to the molecular orbital *i* is expressed by the formula:

$$I_i = \sum_{A,\lambda} P_i(A,\lambda)\sigma(A,\lambda), \quad (1)$$

where $P_i(A,\lambda)$ is the population of the molecular orbital *i* by the atomic orbital λ of atom A, $\sigma(A,\lambda)$ – photoemission cross-section of the atomic orbital (see Table S2 in Online Supplementary Materials).

To calibrate this spectrum, we increased the energies by 6.14 eV, so that the energy of the $17\gamma_6^-$, $13\gamma_7^-$ (5) MO became 20.45 eV and the energy of the $12\gamma_7^-$ (6) MO associated with the O 2*s* AO became 21.6 eV. In this case, in the experimental XPS spectrum of MdO_2 to be measured in the future, the O 1*s*

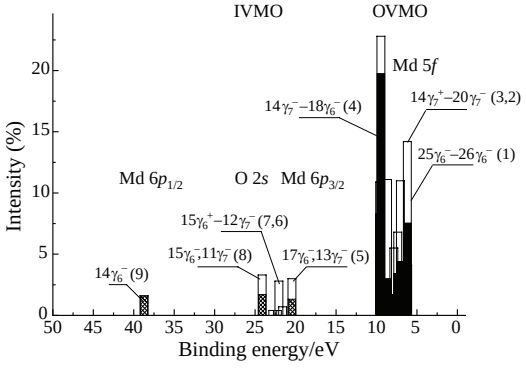

Figure 2 Histogram of the RDV calculated XPS spectrum of MdO_2 (the energy of the exciting X-ray radiation is 1486.6 eV). Filled bars represent Md 5*f* contribution to the MO and shaded bars represent Md 6*p* contribution to the MO.

BE must be E_b(O 1*s*) = 529.9 eV. It is worth mentioning that such calibration for valence XPS spectra unified for all actinide dioxides is necessary to analyze the general regularities of the electronic structure, chemical bonding and the formation of XPS spectra in the AnO_2 row (An = Th–Lr).

The XPS spectrum of MdO_2 can be subdivided into two ranges (Figure 2). The first range from 0 to ~15 eV exhibits the OVMO-related structure, its intensity is mostly attributed to the Md 5*f* and 6*d* electrons. Their photoemission cross-sections are significantly higher than those of the Md 7*s*, 7*p* and O 2*p* electrons (see Table S1 in Online Supplementary Materials).

The second range from ~15 to ~40 eV exhibits the IVMO-related structure. The overlapping in this range occures mostly between the Md 6$p_{3/2}$ and O 2*s* AOs. This range can be subdivided into five components (5–9): $17\gamma_6^-$, $13\gamma_7^-$ (5) 'antibonding' IVMOs; $12\gamma_7^-$ (6), $13\gamma_7^+$, $12\gamma_7^+$, $16\gamma_6^+$ and $15\gamma_6^+$ IVMOs containing the quasiatomic O 2*s* AO; $16\gamma_6^-$ (7) formally 'antibonding' IVMOs; $15\gamma_6^-$, $11\gamma_7^-$ (8) 'bonding' IVMOs; $14\gamma_6^-$ (9) formally 'bonding' IVMO.

The comparison of the configuration of neutral Md atom $6s^26p^65f^{13}6d^07s^27p^0$ with the calculated for MdO_2 in this work $6s^26p^{5.98}5f^{12.44}6d^{1.30}7s^{0.24}7p^{0.54}$ shows that Md effective charge is Q_{Md} = +0.50 e^-. This result reflects an important role of covalent effects in MdO_2. Moreover, the chemical bonding in MdO_2 is more covalent than in ThO_2 since Th effective charge[18] Q_{Th} = 0.93 e^- is higher than Q_{Md} in MdO_2. These results are qualitatively consistent with the data for other actinide dioxides.[21,22] A small effective charge in MdO_2 also agrees with the data on metal–oxide XPS chemical shifts of actinide dioxides: Pu 4$f_{7/2}$ chemical shift between metal Pu and PuO_2 is ΔE_b = 4.0 eV.[12]

To evaluate the contributions of different MOs to the chemical bonding in MdO_2 in the Mulliken approximation, the MO overlap populations were calculated (see Table S3 in Online Supplementary Materials).[21,23] Positive overlap populations indicate the bond strengthening (bonding), while negative overlap populations indicate the bond weakening (antibonding).

The total contribution from OVMOs to bonding population in MdO_2 is 348 (see Table S3 in Online Supplementary Materials). The highest contribution to the bonding strengthening is made by the Md 6*d*–O 2*p* (163), Md 7*p*–O 2*p* (67), Md 6*d*–O 2*s* (43), Md 5*f*–O 2*p* (12) electrons. The electrons of IVMO make the antibonding contribution of –117 in MdO_2. The highest antibonding contribution is made by the Md 6*p*–O 2*p* (–77) electrons. Collectively, the IVMO electrons (–117) weaken the chemical bonding by 34%, while the OVMO electrons (348) strengthen the bonding. The total valence MO contribution to the chemical bonding in MdO_2 is 231 units.

Thus, for the first time, the valence electron density of states in MdO_2 was determined by the RDV method, the MO scheme was constructed and the XPS spectrum of valence electrons was calculated and analyzed in view of the calculated XPS data for valence and core electrons of AnO_2 dioxides (An = Th–Fm). These data are necessary for understanding the features of the chemical bond in MdO_2, for interpreting the complex structure of X-ray spectra (electronic, emission, absorption, conversion, *etc*.) and clarification the general patterns of chemical bond formation in a number of AnO_2 actinide dioxides (An = Th–Lr).

The work was carried out in the framework of the governmental task of the NRC 'Kurchatov Institute' and the state assignment of the Institute of Solid State Chemistry of the Ural Branch of Russian Academy of Sciences (grant no. 124020600024-5).

Online Supplementary Materials

Supplementary data associated with this article can be found in the online version at doi: 10.1016/j.mencom.2024.10.011.

References

1 *The Chemistry of the Actinide and Transactinide Elements*, eds. L. R. Morss, N. M. Edelstein and J. Fuger, 4th edn., Springer, Dordrecht, 2010; https://link.springer.com/book/10.1007/978-94-007-0211-0.
2 K.-N. Huang, M. Aoyagi, M. H. Chen, B. Graseman and H. Mark, *At. Data Nucl. Data Tables*, 1976, **18**, 243; https://doi.org/10.1016/0092-640X(76)90027-9.
3 K. D. Sevier, *At. Data Nucl. Data Tables*, 1979, **24**, 323; https://doi.org/10.1016/0092-640X(79)90012-3.
4 V. G. Yarzhemsky, A. Yu. Teterin, Yu. A. Teterin and M. B. Trzhaskovskaya, *Nucl. Technol. Radiat. Prot.*, 2012, **27**, 103; https://doi.org/10.2298/NTRP1202103Y.
5 V. N. Serezhkin and L. B. Serezhkina, *Radiochemistry*, 2022, **64**, 603; https://doi.org/10.1134/S1066362222050034.
6 A. E. Putkov, Yu. A. Teterin, A. L. Trigub, S. V. Yudintsev, O. I. Stefanovskaya, K. E. Ivanov, S. N. Kalmykov and V. G. Petrov, *Mendeleev Commun.*, 2023, **33**, 135; https://doi.org/10.1016/j.mencom.2023.01.043.
7 B. K. Rai, A. Bretaña, G. Morrison, R. Greer, K. Gofryk and H.-C. Zur Loye, *Rep. Prog. Phys.*, 2024, **87**, 066501; doi: 10.1088/1361-6633/ad38cb.
8 F. A. Pereiro, S. S. Galley, J. A. Jackson and J. C. Shafer, *Inorg. Chem.*, 2024, **63**, 9687; https://doi.org/10.1021/acs.inorgchem.3c03828.
9 F. Legg, L. M. Harding, J. C. Lewis, R. Nicholls, H. Green, H. Steele and R. Springell, *Thin Solid Films*, 2024, **790**, 140194; https://doi.org/10.1016/j.tsf.2023.140194.
10 Yu. A. Teterin, A. E. Putkov, M. V. Ryzhkov, K. I. Maslakov, A. Yu. Teterin, K. E. Ivanov, S. N. Kalmykov and V. G. Petrov, *Mendeleev Commun.*, 2023, **33**, 605; https://doi.org/10.1016/j.mencom.2023.09.004.
11 Yu. A. Teterin and A. Yu. Teterin, *Russ. Chem. Rev.*, 2004, **73**, 541; https://doi.org/10.1070/RC2004v073n06ABEH000821.
12 Yu. A. Teterin, K. I. Maslakov, A. Yu. Teterin, K. E. Ivanov, M. V. Ryzhkov, V. G. Petrov, D. A. Enina and St. N. Kalmykov, *Phys. Rev. B*, 2013, **87**, 245108; https://doi.org/10.1103/PhysRevB.87.245108.
13 A. Rosen and D. E. Ellis, *J. Chem. Phys.*, 1975, **62**, 3039; https://doi.org/10.1063/1.430892.
14 D. E. Ellis and G. L. Goodman, *Int. J. Quantum Chem.*, 1984, **25**, 185; https://doi.org/10.1002/qua.560250115.
15 O. Gunnarsson and B. I. Lundqvist, *Phys. Rev. B*, 1976, **13**, 4274; https://doi.org/10.1103/PhysRevB.13.4274.
16 P. Pyykkö and H. Toivonen, *Acta Acad. Abo., B*, 1983, **43**, 1; https://www.users.abo.fi/htoivone/papers/TablesOfRepresentationAndRotationMatrices.pdf.
17 D. A. Varshalovish, A. N. Moskalev and V. K. Khersonskii, *Quantum Theory of Angular Momentum*, World Scientific, Singapore, 1988; https://books.google.ru/books/about/Quantum_Theory_Of_Angular_Momemtum.html?id=nXcGCwAAQBAJ&redir_esc=y.
18 A. Yu. Teterin, M. V. Ryzhkov, Yu. A. Teterin, K. I. Maslakov, T. Reich and S. L. Molodtsov, *Radiochemistry*, 2009, **51**, 560; https://doi.org/10.1134/S1066362209060022.
19 M. B. Trzhaskovskaya and V. G. Yarzhemsky, *At. Data Nucl. Data Tables*, 2018, **119**, 99; https://doi.org/10.1016/j.adt.2017.04.003.
20 U. Gelius, C. J. Allan, G. Johansson, H. Siegbahn, D. A. Allison and K. Siegbahn, *Phys. Scr.*, 1971, **3**, 237; https://doi.org/10.1088/0031-8949/3/5/008.
21 P. J. Kelly, M. S. S. Brooks and R. Allen, *J. Phys., Colloq.*, 1979, **40**, C4-184; https://doi.org/10.1051/jphyscol:1979458.
22 V. A. Gubanov, A. Rosén and D. E. Ellis, *J. Phys. Chem. Solids*, 1979, **40**, 17; https://doi.org/10.1016/0022-3697(79)90090-8.
23 R. S. Mulliken, *Annu. Rev. Phys. Chem.*, 1978, **29**, 1; https://doi.org/10.1146/annurev.pc.29.100178.000245.

Received: 7th April 2024; Com. 24/7473